chemosensors

Article

Synthesis, Characterization and Sensing Properties of AZO and IZO Nanomaterials

Mokhtar Hjiri [1], Lassaad El Mir [1,2,]* and Salvatore Gianluca Leonardi [3]

[1] Laboratory of Physics of Materials and Nanomaterials Applied at Environment, Faculty of Sciences of Gabes, 6072 Gabes, Tunisia; E-Mail: m.hjiri@yahoo.fr

[2] Al Imam Mohammad Ibn Saud Islamic University (IMSIU), College of Sciences, Department of Physics, Riyadh 11623, Saudi Arabia

[3] Department of Electronic Engineering, Chemistry and Materials Engineering, University of Messina, 98166 Messina, Italy; E-Mail: leonardis@unime.it

* Author to whom correspondence should be addressed; E-Mail: Lassaad.ElMir@fsg.rnu.tn; Tel.: +966-531-448-340; Fax: +966-125-81-584.

Abstract: Al-doped ZnO (AZO) and In-doped ZnO (IZO) nanopowders were prepared by a sol-gel route and subsequent drying in ethanol under supercritical conditions. The morphological and microstructural properties were investigated by transmission electron microscopy (TEM) analysis and X-ray powder diffraction (XRD). The characterization study showed that the AZO and IZO nanoparticles were crystalline and exhibited the hexagonal wurtzite structure. Chemoresistive devices consisting of a thick layer of synthesized nanoparticles on interdigitated alumina substrates have been fabricated and their electrical and sensing characteristics were investigated. The sensor performances of the AZO and IZO nanoparticles for carbon monoxide (CO) were reported. The results indicated that both doped-sensors exhibited higher response and quick response/recovery dynamics compared to a ZnO-based sensor. These interesting sensing properties were discussed on the basis of the characterization data reported.

1. Introduction

The development of gas sensors to monitor the toxic and combustible gases is imperative due to the concerns for environmental pollution and the safety requirements for the industry. In general, sensors provide an interface between the electronic equipment and the physical world typically by converting nonelectrical physical or chemical quantities into electrical signals. Recently, gas sensors based on the semiconducting metal-oxides such as SnO_2 and ZnO [1–5] were found to be very useful for detecting the toxic gases. The fundamental sensing principle relies on the change of conductivity of the sensors when they are exposed to certain target gases at moderate temperatures.

The concept of gas sensors using ZnO thin films was first proposed by Seiyama *et al.* [6]. ZnO is sensitive to many gases of interest like hydrocarbons [4], H_2 [7], oxygen [8,9], H_2O [10], CO [11], NO_2 [12], *etc.*, and has satisfactory stability. Moreover, it is robust, has a rapid response with a possibility of miniaturization. However, it has some drawbacks, as high working temperature, normally between 400 and 500 ℃, poor gas selectivity and comparatively low gas sensitivity [13].

The most popular strategies employed to enhance sensor performance are the control of material morphology in order to increase the effective area of adsorption and the use of additives which act as a catalyzer of the solid–gas reaction, by a chemical or electronic mechanism, thus promoting the improvement of the sensors properties [14].

Recent reports shown that some dopant species, such as Al^{3+} and In^{3+}, improve the sensing properties of ZnO [15,16]. According to literature data, these group-III elements into the ZnO nanostructures act as singly charged donors and supply excess carriers to the conductance band, which will increase the conductance and provide a route to improve the sensing properties of ZnO [17].

In this study, AZO and IZO nanomaterials were synthesized, characterized and tested in the monitoring of low concentration of CO in air. The monitoring of CO is of utmost importance in the environmental control. CO is a gas produced during incomplete combustion and it is toxic at very low concentrations. In confined environments, such as automotive cabin, garage parking or tunnels, high concentrations of this pollutant can create serious hazard for the health and should be continuously monitored and controlled [18]. The concentrations of CO pollutant to be monitored in these ambient are very low, 5–50 ppm [19].

The responses of pure, Al- and In-doped ZnO sensing materials to CO were then examined and compared. Finally, the key factors affecting the sensing performances were studied and discussed here.

2. Experimental Section

2.1. Samples Preparation

AZO and IZO nanoparticles were prepared as previously reported by a sol-gel route using 16 g of zinc acetate dehydrate [$Zn(CH_3COO)_2$ $2H_2O$; 99%] as a precursor in 112 mL of methanol [20–22]. After 10 min of magnetic stirring at room temperature, an adequate quantity of aluminum nitrate-9-hydrate corresponding to [Al]/[Zn] ratios of 0.03 were added to obtain AZO sample and an adequate quantity of indium chloride ($InCl_3$) corresponding to [In]/[Zn] ratios of 0.02 were added to obtain IZO sample. XRF analysis of the samples showed a good agreement, within the experimental error, with the above nominal content. After 15 min under magnetic stirring, the solution was placed in an autoclave and

dried in the supercritical conditions of ethyl alcohol ($T_c = 243$ °C; $P_c = 63.6$ bar) according to protocol reported in the reference [23]. The prepared samples have been then annealed at 400 °C in air for 2 h.

2.2. Characterization

The microstructure of the samples was investigated by XRD (Bruker AXS D8 Advance) using the Cu Kα1 wavelength of 1.5405 Å. The crystallite size, D, was calculated by using the Scherrer's formula [24]:

$$D = \frac{0.9\,\lambda}{B\cos\theta_B} \tag{1}$$

where λ is the X-ray wavelength, θ_B is Bragg diffraction angle and B is the full width at half maximum (FWHM) of the XRD peak.

The morphology of the sample particles was monitored by means of transmission electron microscopy (TEM) tests carried out with a JEM-200CX electron microscope.

2.3. Sensing Test

Sensors were made by printing films (1–10 μm thick) of the nano-powders dispersed in water on alumina substrates (6 mm × 3 mm) with Pt interdigitated electrodes and Pt heater located on the backside. The sensors were then introduced in a stainless steel test chamber for the sensing tests. Electrical measurements were carried out in the temperature range from RT to 400 °C, under a synthetic dry air total stream of 100 sccm, collecting the sensors resistance data in the four point mode. Gases coming from certified bottles can be further diluted in air at a given concentration by mass flow controllers. The concentration of CO target gas was varied from 5 to 50 ppm. A multimeter data acquisition unit Agilent 34970A was used for this purpose, while a dual-channel power supplier instrument Agilent E3632A was employed to bias the built-in heater of the sensor to perform measurements at super-ambient temperatures. The gas response, S, is defined as $S = R_0/R$ where R_0 is the baseline resistance in dry synthetic air (20% O_2 in nitrogen) and R is the electrical resistance of the sensor at different CO concentrations in dry synthetic air.

3. Results and Discussion

3.1. Samples Characterization

X-ray powder diffraction analysis was carried out to investigate the crystal structures of the pure and doped samples. Figure 1a shows the X-ray diffraction (XRD) pattern of as-prepared samples. Diffraction patterns show peaks corresponding to (002), (100), (102), (110) and (101) planes, which indicate that the samples are polycrystallines. All the diffraction peaks match the ZnO hexagonal wurtzite structure [25]. In IZO spectrum, peaks of other secondary phases ($Zn_2In_2O_5$ and In_2O_3) are very weak [26]. XRD pattern of AZO nanoparticles shows the presence of a peak associated to a Zn spinel phase, that is $ZnAl_2O_4$ [27]. It appears that, for the Al-doped ZnO sample, the (100) peak position is shifted at higher 2θ-degree with respect to the (100) peak of pure ZnO and IZO sample. This is in according with the smaller ionic radius of Al^{3+} (0.057 nm) with respect that of Zn^{2+} ion

(0.074 nm) that leads to a reduction in the interlayer spacing of ZnO along the c-axis. The ionic radius of In^{3+} (0.081 nm) is slightly larger than that of Zn^{2+}, and seems do not modify substantially the ZnO lattice.

XRD on samples annealed at 400 °C confirms the presence of wurtzite structure. Interestingly, it can be seen in Figure 1b that the diffraction peaks of both annealed AZO and IZO samples are slightly shifted towards the lower Bragg angle as compared to pure ZnO sample. The peak shift may be attributed to the lattice expansion induced by annealing that leads to an increase in the interlayer spacing of doped-ZnO along the c-axis.

Figure 1. (**a**) X-ray diffraction spectra of as-prepared pure and doped ZnO aerogel nanoparticles. (**b**) Shift detail of (002) and (101) peaks of the samples treated at 400 °C.

(**a**)

(**b**)
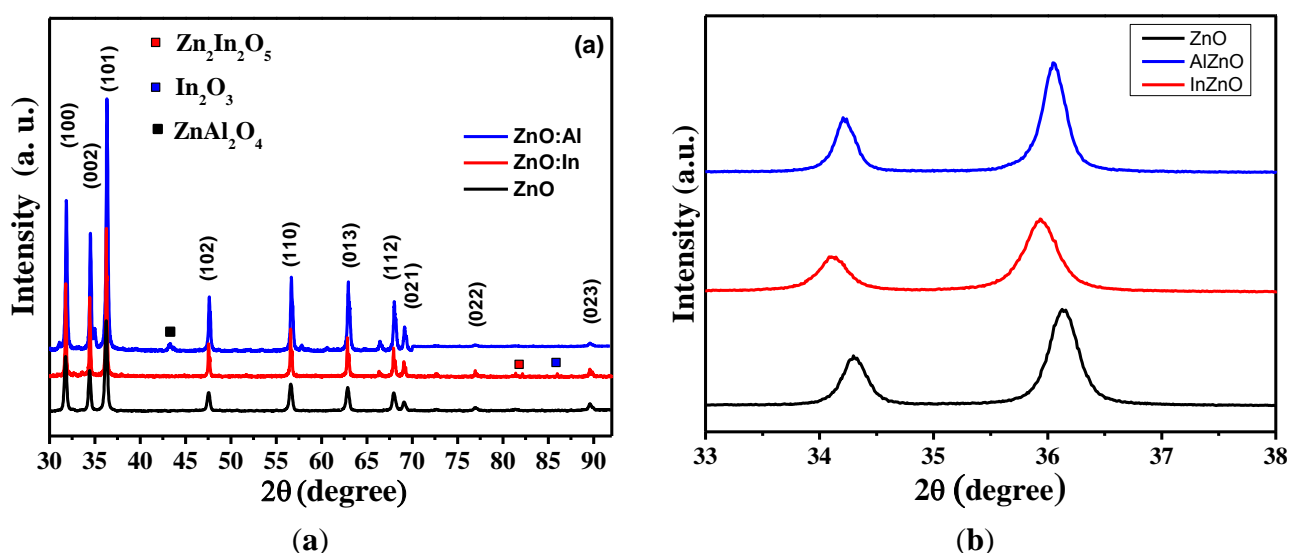
From the XRD measurements, the average crystallite size D, estimated by Scherrer's formula, were 65 nm for pure ZnO, 88 nm for AZO and 58 nm for IZO. The theoretical surface area, SA, was calculated using the equation SA = 6/(D*ρ), where D is the particle size, ρ is the theoretical density of ZnO (5.606 g/cm^3). Values of SA calculated are 16.5, 12.2 and 18.5 m^2/g for ZnO, AZO and IZO, respectively.

Figure 2 reports a typical TEM image taken from the as-prepared samples by sol-gel method and subsequent drying in supercritical conditions. Very small particles having size in the nanometer range are observed. The crystallites present a prismatic-like shape with a narrow particle size distribution. The majority of ZnO particles have a size of about 25–30 nm (Figure 2a). Doped samples show a similar prismatic shape [28]. However, TEM measurements show that the size of the majority of IZO particles varies between 40 and 50 nm [28], whereas the size of AZO particles varies between 20 and 50 nm (Figure 2b). TEM analysis on samples annealed at 400 °C showed that the shape of particles was not modified with respect to as prepared samples, and only an increase of the particle size of ZnO has been noted, which confirms XRD data.

Figure 2. Typical TEM images showing the shape and size of as prepared aerogel nanoparticles. (**a**) ZnO, (**b**) AZO.
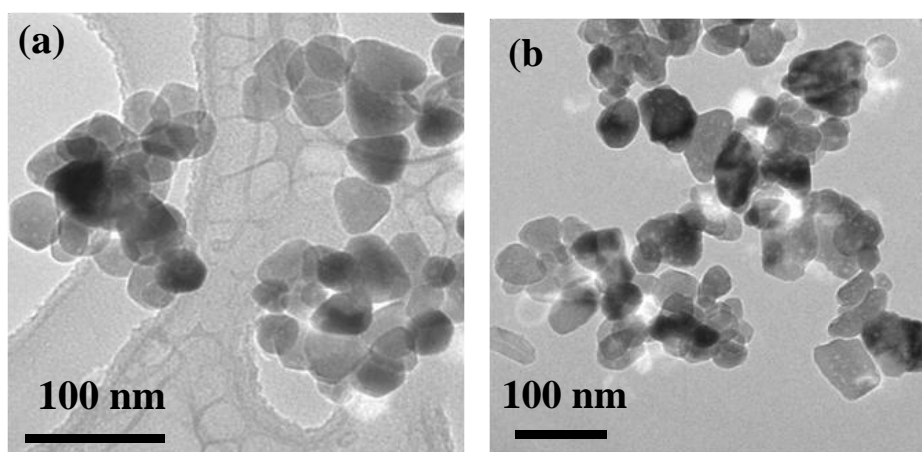
3.2. Sensing Tests

Sensing tests were carried out by means of a home-made sensing probe consisting of an alumina substrate with Pt interdigitated electrodes. On the back side of alumina substrate, a Pt heater provides to the heating of the sensing element. The active sensing layer was deposited on the Pt interdigitated electrodes area from an aqueous paste (in the weight ratio 1:1) of the samples by screen printing. No binder was necessary to enhance the adhesion of the sensing layer on the alumina substrate. After deposition the film was allowed to dry to room temperature and then annealed at 400 °C in air.

Figure 3 summarizes the data obtained, reporting the sensors response to 50 ppm of CO *versus* the operating temperature. The pure ZnO shows a maximum at 250 °C. For doped ZnO, it appears clear that doping favors strongly the sensitivity towards carbon monoxide.

Figure 3. CO response of pure and doped ZnO nanoparticles as a function of the temperature.
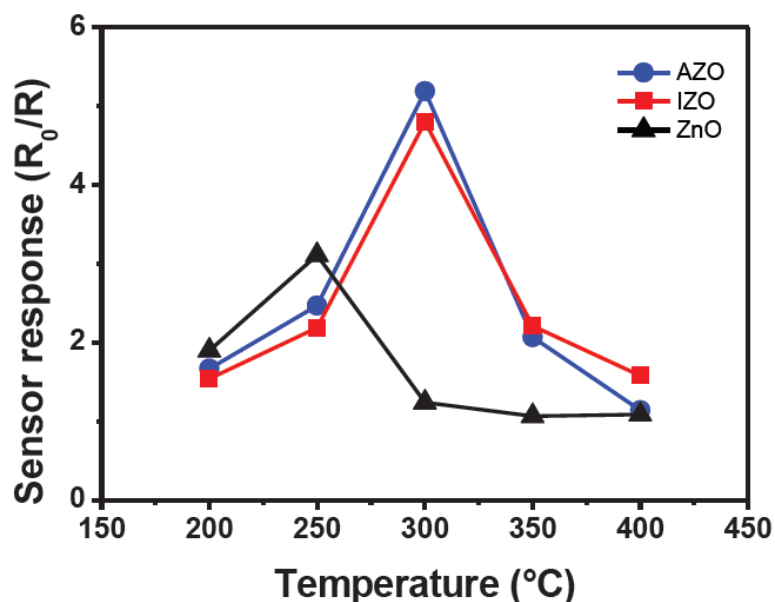
It appears that the sensor response is much dependent on the operating temperatures and the presence of additives. At lower temperature, the increase of the temperature leads an enhancement of sensor response. The responses show a maximum around 300 °C and AZO response is higher than IZO response. At higher temperature, the sensor response gets decreases. Temperature dependence of the sensing properties could result from change of the adsorption and desorption rates of the oxygen ions on the metal-oxide surface. It is well accepted that the sensitivity of semiconductor gas sensors is attributed to the chemisorption of oxygen on the oxide surface and the subsequent reaction between adsorbed oxygen and tested gas, which causes the resistance change. The same mechanism may be applied for the CO sensing of the present AZO and IZO layers. Thus, more CO molecules can react with more oxygen species on the layer grain surface, and can cause the decrease of barrier height leading to the reduction of electrical resistance. Stable oxygen ions species were O_2^- below 100 °C, O^- between 100 and 300 °C, and O^{2-} above 300 °C [29].

The relevant reactions on the surface area could be as follows:

$$2CO + O_2^- \rightarrow 2CO_2 + e^- \tag{2}$$

$$CO + O^- \rightarrow CO_2 + e^- \tag{3}$$

$$CO + O^{2-} \rightarrow CO_2 + 2e^- \tag{4}$$

Reducing agents such as CO will react rapidly with O^- presents on the surface, but very slowly with O_2^-. At temperature below 200 °C, only Equation (2) plays a major role. As a result, a low CO response was achieved at that temperature. At 300 °C, the dominant oxygen species adsorbed on the surface and grain boundaries of the AZO and IZO layers may be O^- and O^{2-} (Equations (3) and (4)). For the gas sensing test performed at temperatures higher than 300 °C, the surface reaction can be represented mainly by Equation (4).

Figure 4 shows the typical transient response of AZO and IZO layers at the operating temperature of 300 °C. It was found that the injection of 50 ppm CO induced a remarkable decrease in electrical resistance of the layer, leading to response magnitude of 4.80 and 5.2 for IZO and AZO sensors, respectively. A similar behavior but with low response is also observed for pure ZnO sample. It is also noted from this figure that the signal could return to its initial value after several cycles. This indicates that the adsorption of CO on the layer surface was reversible. The CO adsorbed on the surface was surely desorbed when CO gas was pumped out. Figure 4d shows transient response recovery for all samples at 5 ppm CO. The sensor responses and recovery time are about 20 s respectively.

Figure 5 reports the response of the fabricated sensors, tested at different CO concentrations and at the operating temperature of 300 °C. Both Al and In dopants lead to an enhancement of the sensors' response towards CO gas. Sensors response found to be obviously changed upon exposure to CO of as low as 5 ppm. At higher CO concentrations, the response was much increased.

Figure 4. Transient responses of the sensors tested to different CO concentrations in air at the operating temperature of 300 °C. (**a**) AZO; (**b**) IZO; (**c**) ZnO; (**d**) Dynamic response comparison.

(**a**)

(**b**)

(**c**)

(**d**)
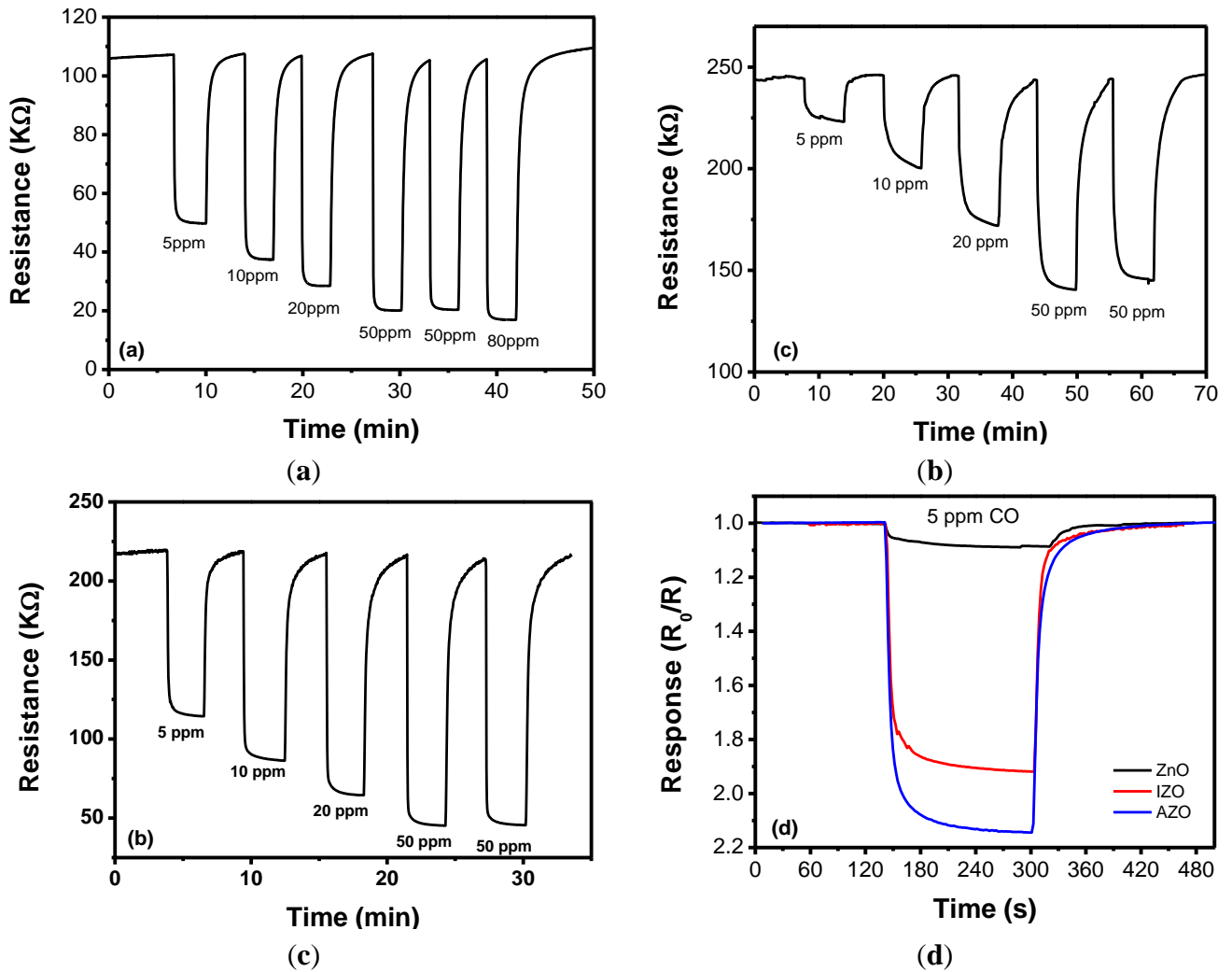
Figure 5. CO response of pure and doped ZnO nanoparticles as a function of CO concentrations.
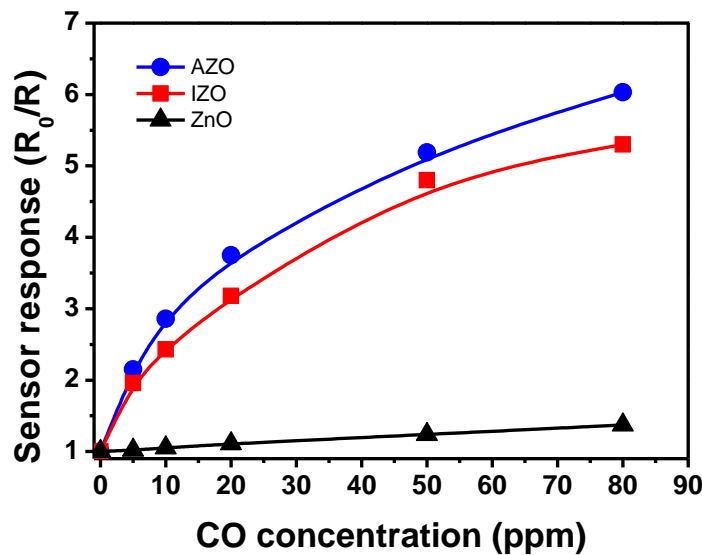
From characterization data of annealed samples, only a little change in the particle size has been evidenced for the annealed doped samples in comparison to pure ZnO sample. Then, it can be excluded that the sensing performances are due to a higher surface area of the doped samples. Instead, the strong improvement in the response to CO by Al and In doping can be attributed to changes to the defect equilibrium in the ZnO crystals by the substitution of Al^{3+} and In^{3+} for Zn^{2+} ions in the ZnO lattice. Oxygen vacancies are the most common defects in semiconductor metal oxides. Zn^{2+} ions in the ZnO lattice are easily substituted by Al^{3+} ions because the ionic radius of Al^{3+} (0.057 nm) is smaller than that of Zn^{2+} ions (0.074 nm). However, to maintain electrical neutrality the positive valence charge of the substituted Zn site has to be compensated by releasing electrons. Thus, electrons are introduced into the doped ZnO samples, which increase the concentration of free electrons, resulting in the decrease in resistance of the oxide. Al doping can modify the surface state, such as by increasing the oxygen vacancies, leading to an enhancement of the gas sensing. Similar considerations can be made for indium doped Zinc oxide. Replacement of the Zn^{2+} cation by the In^{3+}, which acts as donor, reduces the resistivity than pure zinc oxide. Further, indium doping leads to formation of active adsorption sites (indium atoms and oxygen vacancies) which favor the adsorption of oxygen species [30]. Thus, we can draw a conclusion that the defects play an important role in the sensing performance of AZO and IZO sensors.

However, in order to make any meaningful comparison between AZO and IZO and correlate the increase of sensor response to the presence of Al and In in the samples, a quantitative analysis of the surface dopant concentration should be made. As the surface composition could be different from bulk composition, a detailed XPS is planned, finalized to provide helpful indications about surface characteristics of the sensing layer films.

4. Conclusions

In summary, the morphological, microstructural and electrical properties of Al and In-doped ZnO particles prepared by a sol gel method were investigated. The sensing characteristics of chemoresistive sensors prepared were also investigated. The sensors fabricated based on Al-doped ZnO nanoparticles exhibited high sensitivity and very fast response and recovery times. Similar behavior was observed for In-doped ZnO. Our results indicate that the Al-doped ZnO and In-doped ZnO sensors have potential applications in fabricating practical gas sensor devices.

Author Contributions

All authors contributed to this work. Mokhtar Hjiri prepared the samples and wrote the main paper. Gianluca Leonardi built the experimental setup and performed the experiments. Lassaad El Mir supervised the project and edited the manuscript. All authors contributed to the data analysis.

Conflicts of Interest

The authors declare no conflict of interest.

References

1. Chopra, K.L.; Major, S.; Pandya, D.K. Transparent conductors—A status review. *Thin Solid Films* **1983**, *102*, 1–46.
2. Horrillo, M.C.; Gutiérrez, J.; Arés, L.; Robla, J.I.; Sayago, I.; Getino, J. The influence of the tin-oxide deposition technique on the sensitivity to CO. *Sens. Actuators B* **1995**, *25*, 507–511.
3. Sberveglieri, G. Recent development in semiconducting thin film gas sensors. *Sens. Actuators B* **1995**, *23*, 103–109.
4. Jones, A.; Jones, T.A.; Mann, B.; Firth, J.G. The effect of physical from the oxide on the conductivity changes produced by CH_4, CO and H_2O on ZnO. *Sens. Actuators* **1984**, *5*, 75–88.
5. Kohl, D. Surface processes in the detection of reducing gases with SnO_2-based devices. *Sens. Actuators* **1989**, *18*, 71–113.
6. Seiyama, T.; Kato, A.; Fjiishi, K.; Nagatani, M. A New Detector for Gaseous Components Using Semiconductive Thin Films. *Anal. Chem.* **1962**, *34*, 1502–1503.
7. Basu, S.; Dutta, A. Modified heterojunction based on zinc oxide thin film for hydrogen gas-sensor application. *Sens. Actuators B* **1994**, *22*, 83–87.
8. Sberveglieri, G.; Nelli, P.; Groppelli, S.; Quaranta, F.; Valentini, A.; Vasanelli, L. Oxygen gas sensing characteristics at ambient pressure of undoped and lithium-doped ZnO sputtered thin filmd. *Mater. Sci. Eng. B* **1990**, *7*, 63–68.
9. Lampe, U.; Müller, J. Thin-film oxygen sensors made of reactively sputtered ZnO. *Sens. Actuators* **1989**, *18*, 269–284.
10. Traversa, E.; Bearzotti, A. A novel humidity-detection mechanism for ZnO dense pellets. *Sens. Actuators B* **1995**, *23*, 181–186.
11. Hjiri, M.; El Mir, L.; Leonardi, S.G.; Donato, N.; Neri, G. CO and NO_2 Selective Monitoring by ZnO-Based Sensors. *J. Nanomater.* **2013**, *3*, 357–369.
12. Baratto, C.; Sberveglieri, G.; Onischuk, A.; Caruso, B.; di Stasio, S. Low temperature selective NO_2 sensors by nanostructured fibres of ZnO. *Sens. Actuators B* **2004**, *100*, 261–265.
13. Xu, J.; Shun, Y.; Pan, Q.; Qin, J. Sensing characteristics of double layer film of ZnO. *Sens. Actuators B* **2000**, *66*, 161–163.
14. Yamazoe, N. Approaches for improving semiconductor gas sensor. *Sens. Actuators B* **1991**, *5*, 7–19.
15. Hou, Y.; Soleimanpour, A.M.; Jayatissa, A.H. Low resistive aluminum doped nanocrystalline zinc oxide for reducing gas sensor application via sol-gel process. *Sens. Actuators B* **2013**, *177*, 761–769.
16. Paraguay, D.F.; Miki-Yoshida, M.; Morales, J.; Solis, J.; Estrada, L.W. Influence of Al, In, Cu, Fe and Sn dopants on the response of thin film ZnO gas sensor to ethanol vapour. *Thin Solid Films* **2000**, *373*, 137–140.
17. Han, N.; Tian, Y.J.; Wu, X.F.; Chen, Y.F. Improving humidity selectivity in formaldehyde gas sensing by a two-sensor array made of Ga-doped ZnO. *Sens. Actuators B* **2009**, *138*, 228–235.
18. Neri, G.; Bonavita, A.; Micali, G.; Rizzo, G.; Callone, E.; Carturan, G. Resistive CO gas sensors based on In_2O_3 and $InSnO_x$ nanopowders synthesized via starch-aided sol-gel process for automotive applications. *Sens. Actuators B* **2008**, *132*, 224–233.
19. Galatsis, K.; Wlodarski, W. Car cabin air quality sensors and systems. *Encycl. Sens.* **2006**, *8*, 1–11.

20. El Mir, L.; Amlouk, A.; Barthou, C.; Alaya, S. Synthesis and luminescence properties of ZnO/Zn2SiO4/SiO2 composite based on nanosized zinc oxide-confined silica aerogels. *Phys. B* **2007**, *388*, 412–417.

21. El Mir, L.; El Ghoul, J.; Alaya, S.; Ben Salem, M.; Barthou, C.; von Bardeleben, H.J. Synthesis and luminescence properties of vanadium-doped nanosized zinc oxide aerogel. *Phys. B* **2008**, *403*, 1770–1774.

22. El Mir, L.; Amlouk, A.; Barthou, C. Visible luminescence of Al_2O_3 nanoparticles embedded in silica glass host matrix. *J. Phys. Chem. Solids* **2006**, *67*, 2395–2399.

23. El Mir, L.; Ben Ayadi, Z.; Saadoun, M.; von Bardeleben, H.J.; Djessas, K.; Zeinert, A. Optical, electrical and magnetic properties of transparent, n-type conductive $Zn_{0.90-x}V_{0.10}Al_xO$ thin films elaborated from aerogel nanopowder. *Phys. Stat. Sol. (a)* **2007**, *204*, 3266–3277.

24. Cullity, B.D. *Elements of X-ray Diffraction*; Addison-Wesley: Reading, MA, USA, 1978; p. 102.

25. Wienke, J.; van der Zanden, B.; Tijssen, M.; Zeman, M. Performance of spray-deposited ZnO:In layers as front electrodes in thin-film silicon solar cells. *J. Sol. Energy Mater. Sol. Cells* **2008**, *92*, 884–890

26. Singla, M.L.; Shafeeq, M.M.; Kumar, M. Optical characterization of ZnO nanoparticles capped with various surfactants. *J. Lumin.* **2009**, *129*, 434–438.

27. Ben Ayadi, Z.; El Mir, L.; Djessas, K.; Alaya, S. Effect of the annealing temperature on transparency and conductivity of ZnO:Al thin films. *Thin Solid Films* **2009**, *517*, 6305–6309.

28. El-Hilo, M.; Dakhel, A.A. Structural and magnetic properties of Mn-doped ZnO powders. *J. Magn. Magn. Mater.* **2011**, *323*, 2202–2205.

29. Gong, H.; Hu, J.Q.; Wang, J.H.; Ong, C.H.; Zhu, F.R. Nano-crystalline Cu-doped ZnO thin film gas sensor for CO. *Sens. Actuators B* **2006**, *115*, 247–251.

30. Ferro, R.; Rodr ǵuez, J.A.; Bertrand, P. Peculiarities of nitrogen dioxide detection with sprayed undoped and indium-doped zinc oxide thin films. *Thin Solid Films* **2008**, *516*, 2225–2230.